On the use of pulsed DC bias for etching high aspect ratio features

Xingyi Shi, Samaneh Sadighi, Shahid Rauf, Han Luo, Jun-Chieh Wang, Jason Kenney, Jean-Paul Booth, Daniil Marinov, Mickaël Foucher, Nishant Sirse

Journal of Vacuum Science & Technology A

On the Use of Pulsed DC Bias for Etching High Aspect Ratio Features

Xingyi Shi,[1] Samaneh Sadighi,[1] Shahid Rauf,[1] Han Luo, [1] Jun-Chieh Wang,[1] Jason Kenney,[1] Jean-Paul Booth,[2] Daniil Marinov[2], Mickael Foucher[2], and Nishant Sirse[3]

[1]Applied Materials, Inc., 3333 Scott Blvd., Santa Clara, CA 95054, USA
[2]Laboratoire de Physique des Plasma (LPP), CNRS, Sorbonne Université, École Polytechnique, Institut Polytechnique de Paris, 91120 Palaiseau, France
[3]Institute of Science and Research and Centre for Scientific and Applied Research, IPS Academy, Indore-452012, India

[a)] Electronic mail: Xingyi_Shi@amat.com

Inductively coupled plasmas (ICP) containing Cl_2 are widely used for plasma etching in the semiconductor industry. One common issue during plasma etching is aspect ratio dependent etching (ARDE), which is generally attributed to variation in the flux of etchant species to the bottom of features with different dimensions. Insufficient fluxes of neutral etchants to the bottom of high aspect ratio features can also result in sputtering, which tends to distort the feature profile. This article addresses two issues relevant to Cl_2 ICP and plasma etching in these plasmas. First, a comprehensive set of diagnostics is used to validate a model for Cl_2 ICP for gas pressure between 3 – 90 mTorr. The plasma diagnostics include microwave resonant hairpin probe-based measurements of electron density, photolysis-calibrated two-photon laser induced fluorescence (TALIF) measurement of Cl density, photo-detachment-based measurement of Cl^- density, and laser diode absorption spectroscopy of argon metastable species to measure the gas temperature. Consistent with the experiments, the model shows that the electron density peaks near the center of the chamber at low gas pressure due to rapid diffusion. The electron density peak moves under the coils at higher pressures. Using the validated Cl_2

model, we investigate ICPs with rectangular pulsed DC voltage for bias. It is shown that the Cl flux at the bottom of a trench decreases significantly with increasing aspect ratio of the trench. Neutral to ion flux ratio is therefore low at the bottom of higher aspect ratio trenches. The duty cycle of the pulsed bias waveform is found to be an effective means of increasing the neutral to energetic ion flux ratio, which should help with ARDE and sputter reduction.

I. INTRODUCTION

Inductively coupled plasmas (ICP) containing Cl_2 are widely used for plasma etching of semiconductors in the microelectronics industry. One common issue during plasma etching is aspect ratio dependent etching (ARDE) [1], where the etch rate depends on feature aspect ratio. Narrower features, or the same feature at different depths, usually etch more slowly. ARDE is generally attributed to the variation in the flux of etchant species, especially neutral radicals, to the etch front in features of different aspect ratios. It is also well known that the neutral-to-ion flux ratio needs to be high for reactive ion etch [2, 3]. Insufficient neutral flux leads to increased material removal through sputtering. Sputtered byproducts, however, redeposit on feature sidewalls, which reduces the etch rate and distorts the profile. This article addresses two issues relevant to Cl_2 ICP and plasma etching in these plasmas. First, a comprehensive set of diagnostics is used to validate a plasma model for Cl_2 ICP for gas pressure between 3 – 90 mTorr. The measured parameters include electron density (by microwave resonant hairpin probe), Cl atom absolute density (by two-photon laser induced fluorescence (TALIF) with calibration by Cl_2 photolysis), Cl^- negative ion density (by laser photodetachment), and

the gas temperature (from the Doppler width of Argon metastables measured by diode laser absorption spectroscopy). Using the validated Cl_2 model, we investigate ICPs with rectangular pulsed direct current (DC) voltage for bias. It is shown that varying the duty cycle of the pulsed DC bias waveform is an effective means of controlling the neutral to energetic ion flux ratio. The duty cycle of the pulsed DC waveform can therefore be used to control ARDE and feature profiles.

Because of their technological importance, Cl_2 ICPs have been the subject of many experimental and modeling studies. Malyshev *et al.* [4] examined Cl_2 pulsed ICPs using a Langmuir probe and microwave interferometry. They found that an ion-ion plasma forms near the end of the off-period at 10 mTorr and higher pressures. Fleddermann and Hebner [5] used laser photo-detachment and microwave interferometry to measure the density of negative Cl^- ions and electrons. The negative ion density was found to exceed the electron density in a Cl_2 ICP. Donnelly and Malyshev [6] measured the neutral gas temperature in Cl_2 ICPs. The gas temperature was found to be above 1000 K at 20 mTorr and for more than 500 W source power. Donnelly *et al.* [7] estimated the absolute concentrations of Cl_2 and Cl using optical emission spectroscopy by adding trace amounts of rare gases to Cl_2 plasmas. Neuilly, Booth, and Vallier [8] used ultraviolet absorption spectroscopy to measure the chlorine dissociation fraction in Cl_2 ICP. Cl_2 depletion was highest at low pressure and high power in their measurements. Marro and Graham [9] used TALIF to measure atomic Cl density in Cl_2 ICP. They observed almost complete dissociation of Cl_2 molecules at 40 mTorr. Guha, Donnelly, and Pu [10] used mass and Auger electron spectroscopy to look at the interaction of molecular chlorine on anodized Al surface. The surface recombination

coefficient was found to be a function of Cl/Cl_2 density ratio. Cunge *et al.* [11] used laser diode absorption spectroscopy to measure the gas temperature in several gases including Cl_2 in an industrial ICP system. They observed high gas temperatures under most conditions, as well as a temperature jump between the gas and the chamber surface. Bodart *et al.* [12] studied pulsed Cl_2 ICPs and found that the plasma chemistry can be significantly controlled by changing the duty cycle and pulsing frequency. Booth *et al.* [13] and Sirse *et al.* [14] used TALIF to measure the absolute density of atomic Cl in a Cl_2 ICP, using photolysis of Cl_2 to put the values on an absolute scale. They found that the dissociation fraction of Cl_2 decreases with increasing gas pressure. Marinov *et al.* [15] measured the density of Cl_2 in several vibrational states using ultra-broad-band absorption spectroscopy. Their measurement suggested that, despite rapid electron-impact excitation of vibrational levels, the vibrational and translational degrees of freedom in the plasma are close to local equilibrium due to efficient v-T transfer between Cl atoms and Cl_2 molecules.

Cl_2 ICPs have been the subject of several modeling studies in the literature. Park and Economou [16] discussed the modeling of low pressure RF discharges and compared electropositive (Ar) with electronegative (Cl_2) plasmas. The sheath was found to be thinner and the bulk electric field larger in the electronegative plasma. Meeks *et al.* [17] described a model for Cl_2 ICPs. Based on comparison with experiments, they estimated that the Cl recombination rate on anodized-aluminum walls was close to 0.1. Thorsteinsson and Gudmundsson [18] described a global model for Cl_2 plasma. They predicted a high degree of Cl_2 dissociation in the 1 – 100 mTorr gas pressure range. Ventzek, Grappherhaus, and Kushner [19] described a 2-dimensional model for Cl_2 ICP.

They examined issues related to the design of the plasma system focusing on plasma uniformity. Lee and Lieberman [20] described global models for high-density plasmas of several gases including Cl_2. They found the surface recombination to be important in affecting both the degree of dissociation and the Cl^- negative ion density in Cl_2 plasma. Subramonium and Kushner [21] examined pulsed Ar/Cl_2 ICPs. Their simulation results showed high peak electron temperature at low duty cycle, as well as islands of Cl^- forming in the periphery of the reactor due to the slow response of the Cl^- density to pulsed power. Ramamurthy and Economou [22] described a 2-dimensional model for pulsed Cl_2 ICP. The Cl^- density was found to be non-uniform. Corr *et al.* [23] compared fluid simulations of an Ar/Cl_2 ICP with experiments. They fitted the Cl density by adjusting the wall recombination coefficient. The electron density was found to be higher below the quartz window at high pressure. Kemaneci *et al.* [24] used a global model for a Cl_2 high-density plasma to examine pulse modulation, as well as the effect of gas temperature and Cl wall recombination. Despiau-Pujo *et al.* [25] compared a 0D model of pulsed Cl_2/Ar ICP to experiments. The plasma electronegativity was found to increase considerably during the off period.

During Si etching using Cl_2, it is important to have the Si surface sufficiently covered with Cl for the reactive ion etch process to take place efficiently. Chang and Sawin [2] showed that the Cl-to-ion flux ratio must be > 100 before the etch yield becomes insensitive to the ion/neutral flux ratio. Until we get to this regime, either the etch rate is a function of the neutral flux, or sputtering becomes the dominant method for Si removal. Both these scenarios are problematic. If the etch rate is dependent on the magnitude of the Cl flux, features with different sizes etch at different rates, i.e. ARDE

occurs. When there is a Cl deficiency, significant etch slow-down can also be observed during the etching of a high aspect ratio feature. In addition, when the surface is not fully chlorinated and material removal occurs via sputtering, sputtered byproducts can redeposit on sidewalls of high aspect ratio features. Byproduct redeposition leads to tapered sidewalls, twisting, roughness, and slow etch rate. Several approaches can be used to enhance Cl coverage on the feature bottom. One common method is pulsing of the RF bias [26]. RF bias is used to independently control the surface incident ion energy in high-density plasmas. The ratio of the Cl flux to the energetic ion flux can be controlled through the duty cycle of RF bias pulsing. Another method to fully passivate the bottom surface is atomic layer etching (ALE) [27]. In ALE, one temporally separates neutral passivation and reactive ion etch due to energetic ions. The duration of the passivation and etch steps can be used to control the passivation of the feature bottom, as well as ensuring that etching only occurs in the reactive ion etch mode. In this article, we demonstrate that, when a pulsed DC waveform is used for biasing, the duty cycle of the waveform is another effective means to controlling the neutral to energetic ion flux ratio.

This article in organized in the following manner. The experimental system and diagnostics are described in Sec. II. The Cl_2 ICP plasma model and the model used for flux calculation in trenches is discussed in Sec. III. The results are discussed in Sec. IV. A summary is included in Sec. V.

II. EXPERIMENTS

Experimental measurements were made in the INCLINE ICP reactor, described in Booth *et al.* [13]. The plasma was produced in a cylindrical chamber (hard anodized aluminum, 12 cm high, 55 cm diameter) excited by an external 4-turn planar spiral coil through an alumina window. The coil is excited at 13.56 MHz via an L-type match-box and terminated to ground through a 150 pF capacitor to minimize the coil voltage and therefore the amount of capacitive coupling. In the place of a substrate holder there is a bare aluminum plate, 20 cm diameter and 2 cm high above the base plate such that the distance between the dielectric window and the plate is 10 cm. There is no possibility of RF biasing in this experimental setup. Pure Cl_2 gas was flowed through the reactor at 50 sccm, and the pressure was regulated between 1 and 99 mTorr with a throttle valve above the turbo-molecular pump.

The absolute chlorine atom density at the reactor (axial and radial) center was determined by TALIF, as described by Ono *et al.* [28], combined with calibration by photolysis of a known density of Cl_2 gas, as described in Booth *et al.* [13]. Cl atoms in the $^2P^o_{3/2}$ ground state were excited to the $^4S^o_{3/2}$ state by two photons at 233.2 nm (approximately 2 mJ, supplied by a pulsed frequency doubled dye laser pumped with a tripled Nd:YAG laser) focused at the reactor center, and detected by 726 nm fluorescence to the $^4P^o_{5/2}$ state. For absolute density calibration of the TALIF signal, the reactor was filled with 50 mTorr of Cl_2 gas (without plasma) in thermal equilibrium with the reactor walls, and photolyzed (with a well-known cross-section) by a counter-propagating 355 nm laser beam, as described in Booth *et al.* [13].

The electron density was measured using a floating hairpin microwave resonant probe [29]. A tunable microwave signal, suppled via a rigid coaxial cable terminated by a

single-turn loop, enclosed in a glass envelope, was used to excite a tungsten hairpin (length 30 mm) fixed onto the glass envelope by a glass collar, as described in Booth *et al.* [30]. The microwave signal was supplied by a swept microwave source, and the resonance frequency was determined from the minimum in the reflected signal via a directional coupler and Schottky diode. The electron density is calculated from the resonance frequency shift (plasma on – plasma off), including a correction for a floating sheath as described by Piejak *et al.* [31]. The vacuum feedthrough for the microwave input is installed on a translatable vacuum bellows, allowing the probe position to be moved from the reactor center to the radial edge (at a vertical position midway between the dielectric window and the substrate holder).

The Cl^- negative ion density was determined using laser photodetachment at 266 nm, using the same hairpin resonant probe to measure the transient electrons produced. The Cl^- negative ions were photodetached by frequency-quadrupled Nd:YAG laser beam (40 mJ/pulse, 6mm diameter with a top-hat profile passed though the arms of the hairpin probe at about a 10^o angle. The photodetachment cross-section of Cl^- ions at this wavelength is $\sim 13\times10^{-18}$ cm^2, leading to ~90% photodetachment of the Cl^- ions [32]. The time-resolved electron density following the laser pulse was determined by measuring the reflected microwave signal as a function of time for each microwave frequency during a step scan of the frequency, as described by Karkari *et al.* [33]. Measurements were taken at the reactor axial and radial center.

The gas temperature was determined from the Doppler width of diode laser absorption of metastable argon atoms. 5% argon was added to the gas mixture for the gas temperature measurements. Specifically, the $1s_3$ to $2p_2$ transition at 772.42 nm transition

was probed [11], using a tunable Distributed Feed Back (DFB) laser (Toptica DL100). The laser beam passed through the reactor mid-plane, so that the temperature value obtained is an average across the discharge radius, weighted by the density profile of the metastable atoms.

III. MODELLING

A. Plasma simulations

The plasma simulations in this article were made using a 2D fluid plasma model for the inductively coupled plasma (ICP). This model has been described in previous publications, for example in [34] and the references therein. The basic equations and ICP modeling methodology are also outlined in the recent review by Rauf *et al.* [35]. Succinctly, this model includes the continuity equation for all charged and neutral species, the momentum conservation equation for ions, the drift-diffusion approximation for electron flux, the electron energy conservation equation, and the Poisson equation. Starting from the initial conditions (species densities, electron temperature, potential), these equations are integrated in time. Periodically, as described by Rauf *et al.* [35], the inductive electric field is computed by solving the frequency domain Maxwell equations, which is then used to compute the inductive power coupled to the electrons. The coupled plasma simulation and Maxwell equation solution are simulated until both converge to steady-state values. The plasma model is also coupled to a gas flow model, which is redone every time the Maxwell equations are solved. We do not self-consistently solve for gas temperature (T_{gas}) in the plasma model. We have instead used the experimentally

measured T_{gas} in the simulations. As shown in Sec. IV, our measurements indicate that T_{gas} increases considerably with both pressure and power. For conditions where measurements have not been made, T_{gas} is interpolated or extrapolated from available data.

The Cl_2 plasma chemical mechanism used in the plasma simulations is similar to the one in Subramonium and Kushner [21] with a few differences. The dissociation cross-section for Cl_2 ($e + Cl_2 \rightarrow 2\ Cl + e$) is half of the values proposed by Rogoff, Kramer, and Piejak [36]. The Cl recombination coefficient ($Cl \rightarrow ½\ Cl_2$) is assumed to be 0.08 on all surfaces. Also, the ion-ion neutralization rate for the following reactions is $k = 3.5\times10^{-14}(T_{gas}/300)^{0.5}\ m^{-3}s^{-1}$:

$$Cl^- + Cl_2^+ \rightarrow Cl + Cl_2$$

$$Cl^- + Cl^+ \rightarrow 2\ Cl$$

B. Flux simulations

Monte-Carlo based flux simulations are conducted to understand the effects of bias voltage duty cycle and aspect ratio on the amount of Cl and Cl_2^+ flux received at the etch front. Cl particles are launched from the top of the simulation domain with a polar angular distribution defined by a cosine distribution, and Cl_2^+ particles are launched with a polar angular distribution defined by the ion angular distribution functions obtained from the plasma simulations. For any launched particle, when the particle reaches the trench surface, we assume irreversible chemical reaction occurs and the final position of the particle is recorded. Statistics of the final particle position distributions are obtained by launching one million particles for each species. These data are then converted to the

flux values incident at different locations of the trenches. This type of flux calculation does not account for the changes in surface chemistry or geometry that will happen during a real etch process. The flux calculations give the instantaneous distribution of particles within a fixed geometry.

IV. RESULTS AND DISCUSSION

In this section, we first discuss the experimental measurements. The 2-dimensional modeling results for the Cl_2 inductively coupled plasma (ICP) are next described. The computational results are compared to the experiments and analyzed to obtain the ion and neutral fluxes impinging on a wafer placed on the biased electrode. These fluxes are then used to discuss etch loading using flux calculations within trenches of different aspect ratios (AR).

A. Cl_2 ICP experimental measurements

As mentioned in Sec. III, the gas temperature is not computed in the plasma model, but is set to the values obtained from the experiments. We show the experimentally measured T_{gas} as a function of gas pressure and power in Fig. 1(a). T_{gas} increases with both pressure and power, likely due to increased power transfer from the electrons and ions to the neutral gas through collisions. For each pressure and power setting, T_{gas} is assumed to be spatially constant in the plasma in the simulations. Although measurements in the literature [37, 38] show that T_{gas} varies in ICP plasmas spatially, use of a non-uniform T_{gas} is left to future modeling studies where T_{gas} is self-consistently computed. We have plotted the electron density (n_e) at the center of the chamber versus

power and pressure in Fig. 1(b) and the radial distribution of n_e, at 5 cm from the bottom electrode, at several pressures in Fig. 1(c). At the chamber center, n_e increases with pressure from 3 mTorr to ~10 mTorr and then decreases at higher pressures. At a very low pressure (< 3 mTorr), the discharge cannot be sustained. As the pressure increases beyond this threshold for plasma sustenance, the plasma is either produced capacitive or a significant fraction of power is coupled to the plasma (i.e., ions) capacitively. The increase in n_e with pressure in the range of 3 – 10 mTorr is due to more power being coupled to the plasma inductively, increased collisional ionization due to higher neutral density, and slower diffusive electron and ion loss to the walls. The reasons for the observed decrease in n_e at pressures above 10 mTorr is discussed later in this section, when we compared modeling results to experiments. The results for the radial distribution of n_e are also discussed in detail when they are compared to the modeling results.

B. Cl_2 ICP plasma simulation and validation

Computational modeling was performed for the ICP reactor geometry shown in Fig. 2(a). This geometry is based on the reactor used for the experiments. A flat antenna coil is placed on top of a quartz lid. The coils are powered at 10 MHz. Cl_2 flows into the chamber from the showerhead ring at the top, and the effluent is pumped out at the bottom. The bottom electrode is optionally biased using the pulsed DC voltage waveform shown in Fig. 2(b). The duty cycle of the bias voltage is varied in this study, but the minimum and maximum voltages are kept constant. The bias voltage is assumed to be directly applied to the electrode without a blocking capacitor or dielectric

electrostatic chuck (ESC), so the waveform in Fig. 2(b) appears at the electrode without distortion.

The Cl_2 plasma was modeled in this reactor for a range of gas pressures and bias duty cycles. As the bias voltage amplitude is modest (V_{pp} = 125 V), the plasma properties are primarily dictated by the inductive power coupling from the coil. ICP plasma behavior is well-documented in the literature, so we only show important plasma properties here that are linked to model validation and discussion of ARDE during etching. The gas pressure has a significant influence on the plasma. Inductive power is coupled to the electrons below the coils, which heats the electrons and sustains the discharge. The steady-state electron temperature profiles (T_e) are shown in Fig. 3 at 5 and 50 mTorr gas pressure. Other conditions in the Cl_2 plasma are 500 W ICP power and no bias voltage. Based on the experimental measurements, T_{gas} is set to 700 K at 5 mTorr and 1300 K at 50 mTorr. T_e is highest under the coils in the region where power is coupled to the electrons. Electron thermal conduction is strong at 5 mTorr so T_e is relatively uniform in the chamber. The maximum T_e is lower at 50 mTorr and is less uniform due to the lower thermal conductivity.

The gas pressure also has a major influence on charged and neutral species densities. We have plotted the densities of electrons (n_e), Cl_2^+ positive ions (n_{Cl2+}), and Cl^- negative ions (n_{Cl-}) in Fig. 4, and the Cl density (n_{Cl}) in Fig. 5 for 5 and 50 mTorr. The other conditions in the Cl_2 plasma are 500 W ICP power and no bias voltage. Even though the inductive power is deposited under the coils, diffusion is strong at 5 mTorr, and the electron density peaks at the chamber center. Diffusion is reduced at 50 mTorr, resulting in the n_e peak occurring at the region of peak power deposition. Although the peak n_e is

higher at 50 mTorr, n_e is lower at the chamber center and near the bottom electrode. The plasma is moderately electronegative under the conditions examined, and the peak Cl^- density is comparable or higher than the electron density. As negative ions are less mobile than electrons, the peak in Cl^- remains in the region of highest plasma potential (coincident with the location where the power is deposited) even at 5 mTorr. Due to the presence of these negative ions, the Cl_2^+ density also peaks off-center at both 5 and 50 mTorr. The principal product of dissociation of Cl_2 is Cl atoms. The densities of positive and negative ions are several orders of magnitude lower than that of the Cl density (Fig. 5). The Cl density at 5 and 50 mTorr is shown in Fig. 5 at 5 and 50 mTorr. The Cl density is higher at 50 mTorr due to the higher Cl_2 density. The Cl density peaks near the chamber center at 5 mTorr, but peaks near the location of peak power deposition at 50 mTorr.

One of the goals of the present study is to compare the modeling results to experimental measurements. The electron density was measured 5 cm above the bottom electrode as a function of radius using the hairpin probe. The numerically calculated and experimentally measured n_e for pressures ranging between 10 mTorr and 90 mTorr are shown in Figures 6(a) and 6(b) respectively. These results are for Cl_2 plasma at 500 W ICP power and no bias power. Although there are quantitative differences between the measurements and experiments, the model captures the experimentally observed trends. n_e at the reactor center is highest at 10 mTorr and gradually decreases with increasing pressure. As the gas pressure increases from 10 mTorr, the peak in n_e moves from the chamber center to an off-axis location, due to reduced diffusion at higher pressure. As shown in Fig. 4(a) and Fig. 4(b), the spatial distribution of the electron density shifts with

increasing pressure. At 5 mTorr, the maximum electron density is located at the center of the reactor. This distribution is a result of electron loss to the reactor walls and fast electron diffusion at low pressure. In contrast, at 50 mTorr, the peak electron density is located beneath the coils, where electrons are generated. The variation in the spatial distribution of n_e at different pressures leads to an off-center radial maximum in n_e at 5 cm above the wafer (Fig. 6(a)).

As shown in Fig. 1(b), the experiments show that n_e peaks at around 10 mTorr and decreases at lower pressures. We compare the computed n_e at the chamber center and 5 cm below the dielectric lid to measurement in Fig. 6(c) to illustrate the model behavior at pressures below 10 mTorr. Although n_e does eventually decrease with lowering pressure, the pressure for peak n_e is lower in the model compared to experiment. Based on the modeling results, the decrease at lower pressures is due to faster electron loss to the walls, as well as the reduced number of ionizing collisions with decreasing gas pressure. For very low pressures, it is difficult to sustain the discharge due to lower ionization rate and increased loss. Although there can be several reasons why the peak n_e occurs at lower pressure in the model vs. experiments, one likely reason is that the ICP model ignores capacitive coupling from the coils. A high voltage on the coils at sub – 10 mTorr pressures could result in a significant fraction of the power being deposited capacitively, which mostly couples to ions and does not efficiently produce electrons. At high pressures, the simulated n_e falls off faster with pressure than in the experiments. We suspect that the major reasons for this disparity are (a) the fluid plasma model does not capture non-local electron transport and heating and (b) the scaling of transport coefficients with pressure might be inaccurate.

Although the electron density was measured as a function of chamber radius, the Cl^- and Cl densities were only measured at the chamber center. We have compared measured and computed densities of Cl^- and Cl at R = 0 and 5 cm from the dielectric lid in Fig. 7. These results are plotted from 3 – 90 mTorr. The model captures the general trends and the densities are in the right range. However, there are some notable differences. Both the model and experiment show that n_e peaks at an intermediate pressure range and falls off at lower and higher pressures. Based on the modeling results, the decrease at lower pressures is due to faster electron loss to the walls, as well as the reduced number of ionizing collisions with decreasing gas pressure. For very low pressures, it is difficult to sustain the discharge due to lower ionization rate and increased loss. Although there can be several reasons why the peak n_e occurs at lower pressure in the model vs. experiments, one likely reason is that the ICP model ignores capacitive coupling from the coils. A high voltage on the coils at sub 10 mTorr pressures could result in a significant fraction of the power being deposited capacitively, which mostly couples to ions and does not efficiently produce electrons. At higher pressures, ionization occurs under the coil, and does not diffuse fully to the chamber center. The simulated n_e falls off faster with pressure at this location than in the experiments. Although there can be many reasons for this discrepancy, we suspect that the major reasons are that the fluid plasma model does not capture non-local electron transport and heating, and the scaling of transport coefficients with pressure might be inaccurate. The model shows that the Cl^- density at the chamber center decreases with increasing pressure. More Cl^- is produced at lower pressure, due to the higher electron density and higher T_e. The experimental measurements are in the same range but show a less clear

dependence on gas pressure. The simulated trend of Cl^- density with pressure is consistent with the experimental measurements at 300 W, but shows a more marked decrease with pressure. The Cl density increases with pressure in both the measurements and the modeling results. The measured Cl density increases faster with pressure than the model. Besides the issues pointed out for electron density above, there may be inadequacies in our Cl_2 plasma chemical mechanism. Non-uniform gas temperature might also contribute to this discrepancy.

C. Cl_2 ICP plasma simulation with bias

The results discussed thus far are without bias. We next apply bias voltage with the waveform shown in Fig. 2(b) at the lower electrode. The ICP power in the Cl_2 plasma is 500 W and the gas pressure is 10 mTorr. We ran simulations where the duty cycle was varied between 10 – 90%. Due to low voltage amplitude, the plasma properties, including charged and neutral species' densities and fluxes, were not changed significantly by the application of a bias voltage. We show the ion energy distribution function (IEDF) as a function of duty cycle in Fig. 8. Two peaks can be observed, one near 10 eV and another near 100 eV. At 10% duty cycle, only the low energy peak is prominent. As the duty cycle is increased, the low energy peak decreases, and the peak at the high energy increases in amplitude. Varying the duty cycle is, therefore, a good method to control the relative fractions of low and high energy ions. The high energy peak at 10% duty cycle is broad and at lower energy. This is because of the finite ion transit time, which does not allow full establishment of the sheath during the short time

when bias voltage was -100 V. Similarly, at 90% duty cycle, the sheath did not fully collapse, and the minimum ion energy did not decrease to ~ 10 eV.

As the bias voltage is low, it does not significantly impact the densities or fluxes of species. To illustrate this, we have plotted the flux of atomic Cl and Cl_2^+ ions as a function of duty cycle in Fig. 9. The ion flux is split into 2 groups: those with energy < 50 eV and those at higher energy. These results are for 10 mTorr gas pressure and 500 W ICP power. The fluxes peak at the chamber center for all conditions due to ample diffusion and the relatively large gap. When the duty cycle is 10%, most ions are below 50 eV, but the fraction of high-energy ions is greater than 10%, due to the transition times. As the duty cycle is increased, the proportion of high energy ions increases while the low energy ion fraction decreases. At 90% duty cycle, the sheath does not collapse fully, so there is a negligible number of ions below 50 eV.

D. Effect of duty cycle on loading

The flux ratio of Cl to Cl_2^+ ($\Gamma_{Cl}/\Gamma_{Cl2+}$) at the etch front controls the etch rate and etching profile [2, 3]. To understand the effect of bias voltage duty cycle on this flux ratio, flux calculations are conducted to obtain $\Gamma_{Cl}/\Gamma_{Cl2+}$ for silicon trenches with aspect ratio of 0.1, 1, 10, and 100 and with a constant opening width of 10 nm. Figure 10 shows the value of Γ_{Cl} incident on the four rectangular trenches. We assumed that the sticking coefficient of Cl on Si is unity. In other words, once a Cl atom reaches the trench surface, it is assumed that an irreversible chemical reaction will occur, and the Cl particle trajectory will terminate at that location. The color along the trench edge represents the common logarithm of the normalized flux: $\log_{10}(\Gamma_{Cl}(x,z)/\Gamma_{Cl\ from\ plasma})$. Figure 10(a)

shows that, for a trench with an aspect ratio of 0.1, Γ_{Cl} across the trench is nearly uniform. As the aspect ratio is increased to 10 and 100 Figs. 10(c) and 10(d), Γ_{Cl} on the sidewall decreases with depth. The numbers labelled at the bottom of the four panels indicate the value of the normalized Cl flux ($\Gamma_{Cl\ bottom}/\Gamma_{Cl\ from\ plasma}$) received at the bottom of each of these features. As the aspect ratio increases, the amount of Cl flux received at the trench bottom decreases due to geometric shadowing.

We now examine the fluxes of Cl and Cl_2^+ to the bottom of the four trenches, which represent the location of the etch front. Figure 11(a) shows the trench bottom Cl flux normalized to the plasma-phase Cl flux. When the aspect ratio is increased by a thousand-fold, the value of the Cl flux received decreases by more than two orders of magnitude. For aspect ratios of one and above, there is only a small spatial variation in the Cl flux received across the horizontal surface. The jagged flux reading for aspect ratio of 100 is due to the random nature of the Monte-Carlo technique.

Figure 11(b) shows the normalized ion flux received at the feature bottom for different bias voltage duty cycles. Only ions with energy higher than 50 eV are accounted for. It is also assumed that Cl_2^+ ions have a sticking coefficient of unity. At 90% and 70% duty cycles, the ion flux received at the bottom of the four AR trenches are independent of the aspect ratio. The narrow ion angular distribution for the high energy ion population contributes to this insensitivity to the aspect ratio. As the duty cycle is decreased, there is an increase in the population of relatively lower energy ions with a wider angular spread, which contribute to the slightly lower ion flux for the AR100 geometry (red, black, and blue dotted lines). Finally, as the duty cycle is increased, the flux of 50 eV+ ions landing at the feature bottom increased.

Figure 12 gives a summary of the combined effects of duty cycle and AR on the etch front $\Gamma_{Cl}/\Gamma_{Cl2+}$, where "etch front" refers to the bottom of the four features introduced in Fig. 10. For all aspect ratios, an increase in duty cycle leads to a decrease in the neutral-to-ion flux ratio, due to an increase in the flux of high energy ions. For all duty cycles, an increase in AR will lead to a decrease in the etch front $\Gamma_{Cl}/\Gamma_{Cl2+}$. This trend is the result of the high aspect ratio reducing the Cl flux to the bottom of the features. From this simple case study, one may consider leveraging bias voltage duty cycle to obtain better control of the neutral-to-ion flux ratio during high aspect ratio etching processes.

In general, to reduce the effect of ARDE, one endeavors to ensure the etch front neutral to ion flux ratios for all features is in the plateau region of the etch yield versus neutral to ion flux ratio curve (see Figure 4 in [3]). Depending on the material being etched, the ion energy and angular distributions, and the presence of other chemical species, the ideal neutral to ion flux ratio will vary. In this work, we demonstrate that reducing duty cycle can lead to increasing neutral to ion flux ratio at the etch front. In practice, simultaneous optimization of operating parameters such as source power, pressure, and bias voltage waveform will be necessary to meet the ever-stringent demands on feature profile control.

V. SUMMARY AND CONCLUSIONS

Plasma diagnostics, 2-dimensional modeling, and issues relevant to etching using pulsed DC biasing in a Cl_2 ICP are discussed in this article. A comprehensive set of diagnostics is used to characterize a Cl_2 ICP in the 3 – 90 mTorr pressure range. The

plasma diagnostics include microwave resonant hairpin probe-based measurements of electron density, TALIF measurement of Cl density, photo-detachment-based measurement of Cl^- density, and laser diode absorption spectroscopy of argon metastable species to measure the gas temperature. These diagnostic measurements are used to validate a 2D fluid model of the Cl_2 ICP. The model used the experimentally measured gas temperature. Consistent with the experiments, the model shows that the electron density peaks near the center of the chamber at low gas pressure due to rapid diffusion. The electron density peak moves under the coils at higher pressures. The plasma is moderately electronegative at the center of the chamber and the density of electrons and Cl^- negative ions decreases with pressure. The Cl density increases with gas pressure due to the higher density of Cl_2. Using the validated Cl_2 model, we investigate ICPs with rectangular pulsed DC voltage for bias. It is shown that the Cl flux at the bottom of a trench decreases significantly with increasing aspect ratio of the trench. The neutral-to-ion flux ratio is therefore low at the bottom of higher aspect ratio trenches. The duty cycle of the pulsed bias waveform is found to be an effective means of increasing the neutral to energetic ion flux ratio, which should help with ARDE and sputter reduction.

ACKNOWLEDGEMENTS

Dr. N. Sirse is supported by the Science and Engineering Research Board (SERB) Core Research Grant No. CRG/2021/003536.

AUTHOR DECLARATIONS

Conflicts of Interest *(required)*

The authors have no conflicts to disclose.

DATA AVAILABILITY

Data available on request from the authors.

REFERENCES

1 S. L. Lai, D. Johnson, and R. Westerman, J. Vac. Sci. Technol. A 24, 1283 (2006).

2 J. P. Chang and H. H. Sawin, J. Vac. Sci. Technol. A 15, 610 (1997).

3 C. M. Huard, Y. Zhang, S. Sriraman, A. Paterson, and M. J. Kushner, J. Vac. Sci. Technol. A 35, 05C301 (2017).

4 M. V. Malyshev, V. M. Donnelly, J. I. Colonell, and S. Samukawa, J. Appl. Phys. 86, 4813 (1997).

5 C. B. Fleddermann and G. A. Hebner, J. Vac. Sci. Technol. A 15, 1955 (1997).

6 V. M. Donnelly and M. V. Malyshev, Appl. Phys. Lett. 77, 2467 (2000).

7 V. M. Donnelly, M. V. Malyshev, M. Schabel, A. Kornblit, W. Tai, I. P. Herman, and N. C. M. Fuller, Plasma Sources Sci. T. 11, A26 (2002).

8 F. Neuilly, J.-P. Booth, and L. Vallier, J. Vac. Sci. Technol. A 20, 225 (2008).

9 F. G. Marro and W. G. Graham, Plasma Sources Sci. T. 17, 015007 (2008).

10 J. Guha, V. M. Donnelly, and Y. Pu, J. Appl. Phys. 103, 013306 (2008).

11 G. Cunge, R. Ramos, D. Vempaire, M. Touzeau, M. Neijbauer, and N. Sadeghi, J. Vac. Sci. Technol. A 27, 471 (2009).

12 P. Bodart, M. Brihoum, G. Cunge, O. Joubert, and N. Sadeghi, J. Appl. Phys. 110, 113302 (2011).

13 J.-P. Booth, Y. Azamoum, N. Sirse, and P. Chabert, J. Phys. D Appl. Phys. 45, 195201 (2012).

14 N. Sirse, J.-P. Booth, P. Chabert, A. Surzhykov, and P. Indelicato, J. Phys. D Appl. Phys. 46, 295203 (2013).

15 D. Marinov, M. Foucher, E. Campbell, M. Brouard, P. Chabert, and J.-P. Booth, Plasma Sources Sci. T. 25, 035019 (2016).

16 S.-K. Park and D. J. Economou, J. Appl. Phys. 68, 3904 (1990).

17 E. Meeks, J. W. Shon, Y. Ra, and P. Jones, J. Vac. Sci. Technol. A 13, 2884 (1990).

18 E. G. Thorsteinsson and J. T. Gudmundsson, Plasma Sources Sci. T. 19, 015001 (1990).

19 P. L. G. Ventzek, M. Grapperhaus, and M. J. Kushner, J. Vac. Sci. Technol. B 12, 3118 (1994).

20 C. Lee and M. A. Lieberman, J. Vac. Sci. Technol. A 13, 368 (1995).

21 P. Subramonium and M. J. Kushner, J. Vac. Sci. Technol. A 20, 325 (2002).

22 B. Ramamurthi and D. J. Economou J. Vac. Sci. Technol. A 20, 467 (2002).

23 C. S. Corr, E. Despiau-Pujo, P. Chabert, W. G. Graham, F. G. Marro, and D. B. Graves, J. Phys. D Appl. Phys. 41, 185202 (2008).

24 E. Kemaneci, E. Carbone, J.-P. Booth, W. Graef, J. van Dijk, and G. Kroesen, Plasma Sources Sci. T. 23, 045002 (2014).

25 E. Despiau-Pujo, M. Brihoum, P. Bodart, M. Darnon, and G. Cunge, J. Phys. D Appl. Phys. 47, 455201 (2014).

26 A. Agarwal, P. J. Stout, S. Banna, S. Rauf, K. Tokashiki, J. Y. Lee, and K. Collins, J. Appl. Phys. 106, 103305 (2009).

27 S. D. Park, K. S. Min, B. Y. Yoon, D. H. Lee, G. Y. Yeom, Jpn. J. Appl. Phys. 44, 389 (2005).

28 K. Ono, T. Oomori T, M. Tuda, and N. Namba, J. Vac. Sci. Technol. A 10, 1071 (1992).

29 R. B. Piejak, J. Al-Kuzee and N. St. J. Braithwaite, Plasma Sources Sci. T. 14, 734 (2005).

30 J.-P. Booth, G. Curley, D. Marić, and P. Chabert, Plasma Sources Sci. T. 19, 015005 (2009).

31 R. B. Piejak, V. A. Godyak, R. Garner, B. M. Alexandrovich, and N. Sternberg, J. Appl. Phys. 95, 3785 (2004).

32 A. Mandl, Phys. Rev. A 14, 345 (1976).

33 S. K. Karkari, C. Gaman, A. R. Ellingboe, I. Swindells and J. W. Bradley, Meas. Sci. Technol. 18, 2649 (2007).

34 A. Agarwal, K. Bera, J. Kenney, A. Likhanskii, S. Rauf, J. Phys. D Appl. Phys. 50, 424001 (2017).

35 S. Rauf, K. Bera, J. Kenney, P. Kothnur, J. Micro/Nanopatterning, Mater. Metrol. 22, 041503 (2023).

36 G. L. Rogoff, J. M. Kramer, R. B. Piejak, IEEE T. Plasma Sci. 14, 103 (1986).

37 G. A. Hebner, J. Appl. Phys. 80, 2624 (1996).

38 H. Abada, P. Chabert, J.-P. Booth, J. Robiche, and G. Cartry, J. Appl. Phys. 92, 4223 (2002).

FIGURES AND CAPTIONS

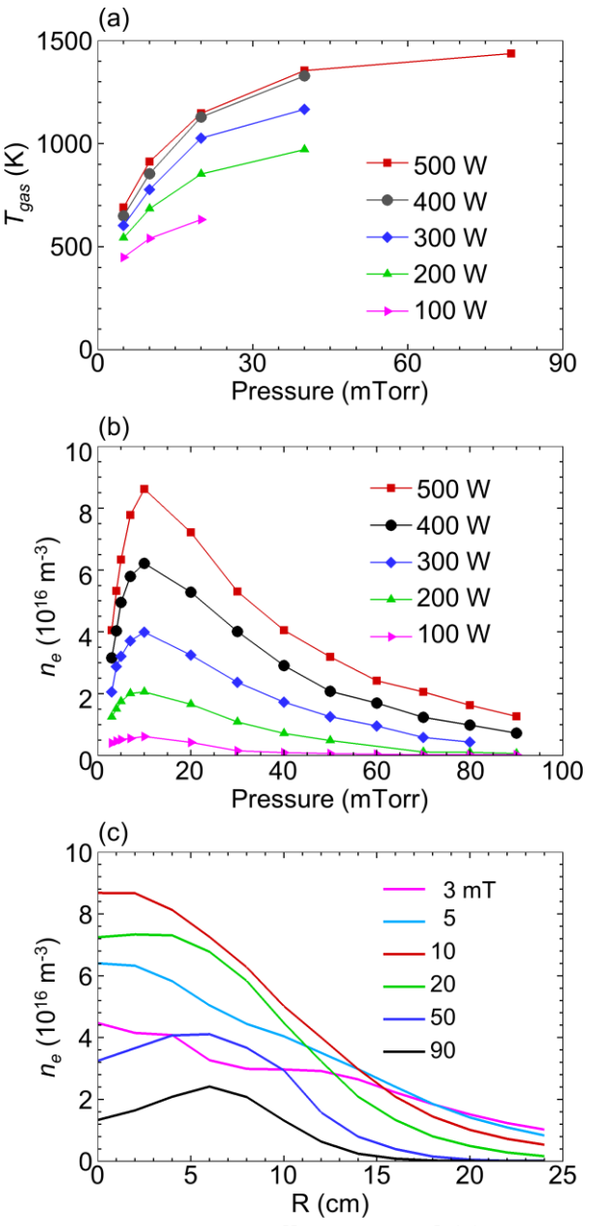

Figure 1. Experimentally measured (a) gas temperature T_{gas} at the radial and axial center of the chamber, (b) electron density n_e at the radial and axial center of the chamber, and (c) n_e vs. radius 5 cm from the dielectric lid.

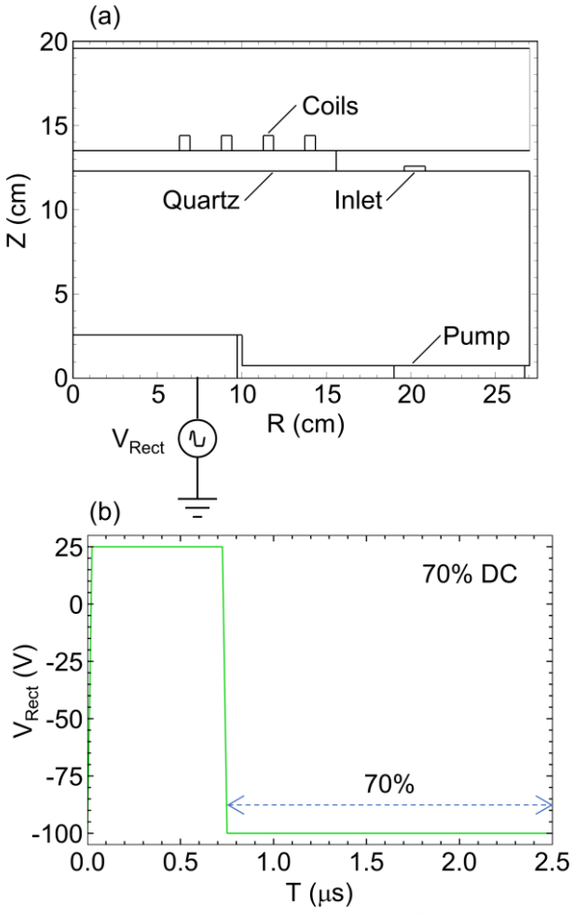

Figure 2. (a) Schematic of the inductively coupled plasma reactor. (b) Pulsed DC bias voltage V_{Rect} is applied to the bottom electrode in some simulations.

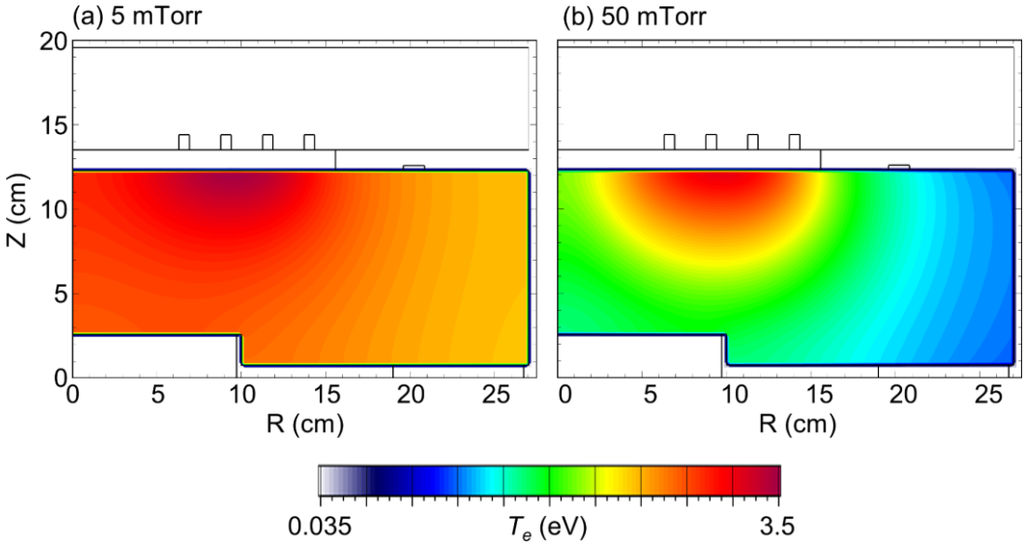

Figure 3. Electron temperature (T_e) at (a) 5 and (b) 50 mTorr. Other conditions are Cl_2 plasma, 500 W ICP power, and no bias voltage. Gas temperature is 700 K at 5 mTorr and 1300 K at 50 mTorr.

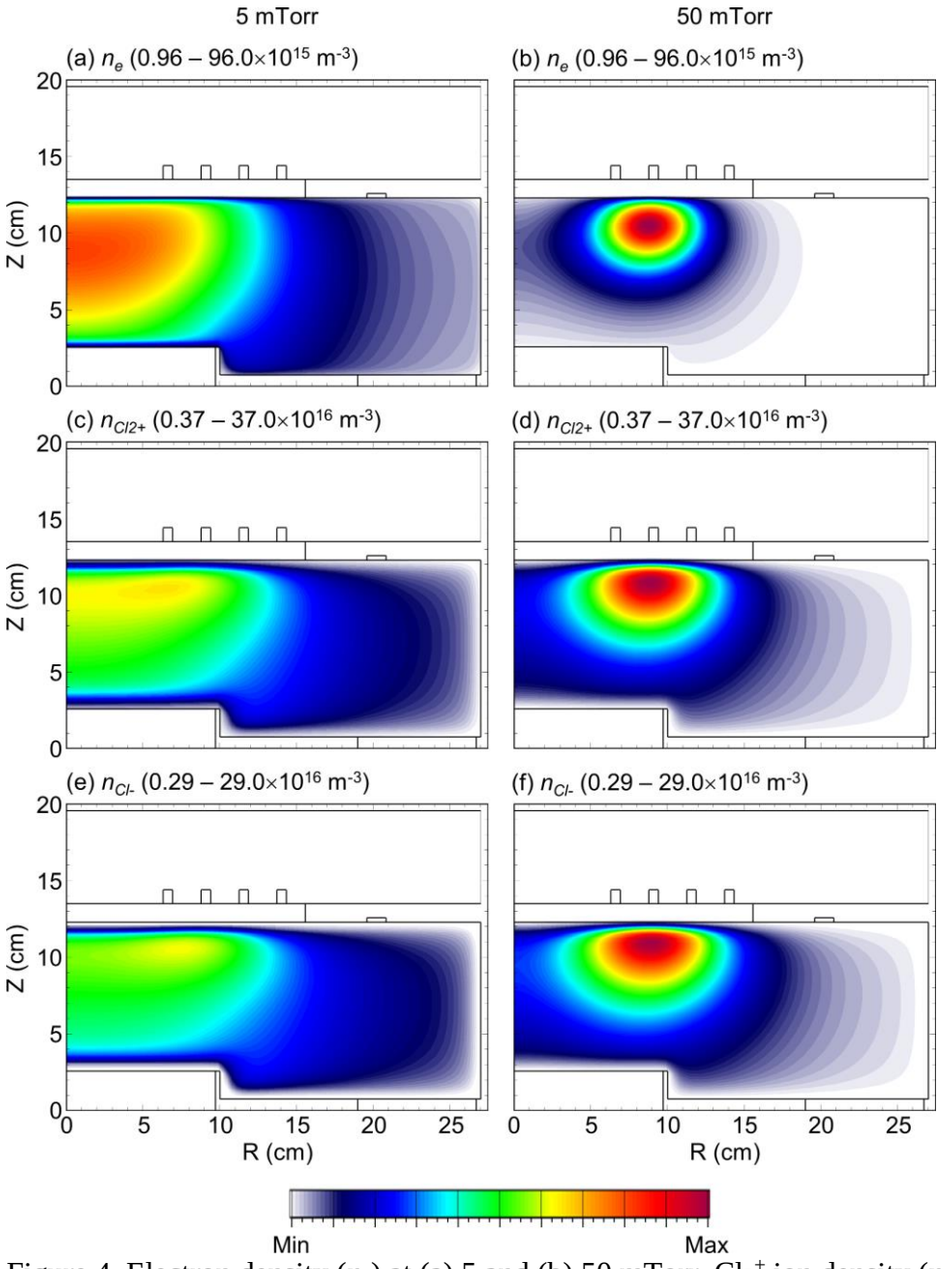

Figure 4. Electron density (n_e) at (a) 5 and (b) 50 mTorr, Cl_2^+ ion density (n_{Cl2+}) at (c) 5 and (d) 50 mTorr, and Cl^- negative ion density (n_{Cl-}) at (e) 5 and (f) 50 mTorr. Other conditions are Cl_2 plasma, 500 W ICP power, and no bias voltage. Gas temperature is 700 K at 5 mTorr and 1300 K at 50 mTorr.

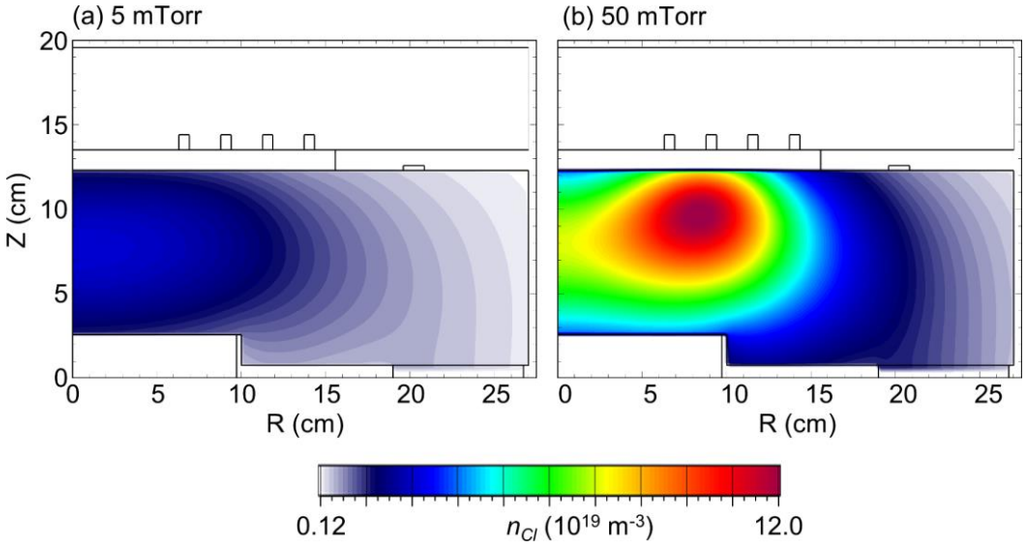

Figure 5. Cl density (n_{Cl}) at (a) 5 and (b) 50 mTorr. Other conditions are Cl_2 plasma, 500 W ICP power, and no bias voltage. Gas temperature is 700 K at 5 mTorr and 1300 K at 50 mTorr.

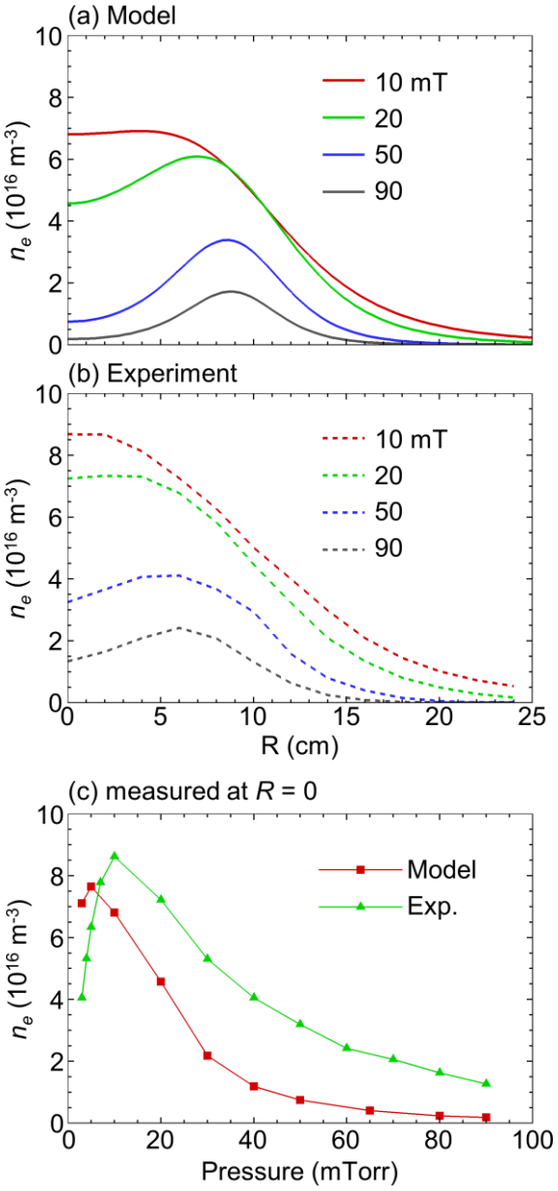

Figure 6. Effect of gas pressure on electron density (n_e) 5 cm below the dielectric lid. The results as a function of radius are from the (a) model and (b) diagnostic measurements. Modeling and experimentally measured n_e at R = 0 is compared in (c). These results are for Cl_2 plasma at 500 W ICP power and no bias voltage.

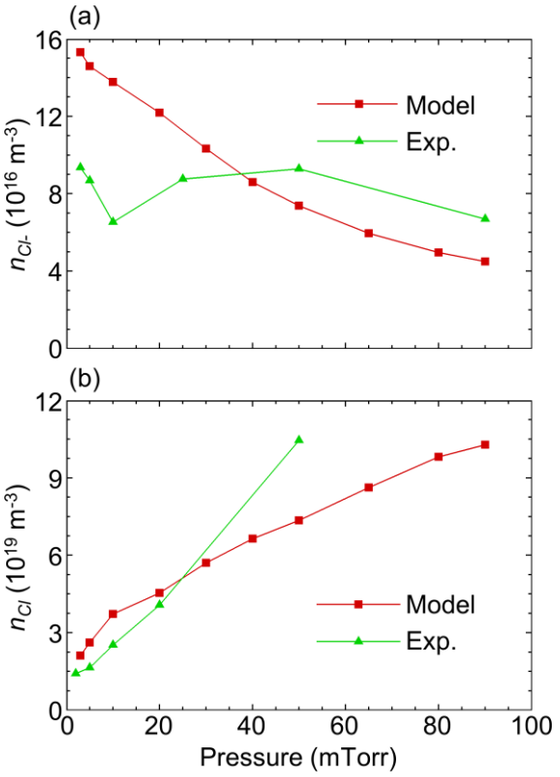

Figure 7. Effect of gas pressure on (a) Cl^- negative ion density (n_{Cl^-}) and (b) Cl density (n_{Cl}). Modeling results are compared to diagnostic measurements. The data has been measured at R = 0 and 5 cm below the dielectric lid. These results are for Cl_2 plasma at 500 W ICP power and no bias voltage.

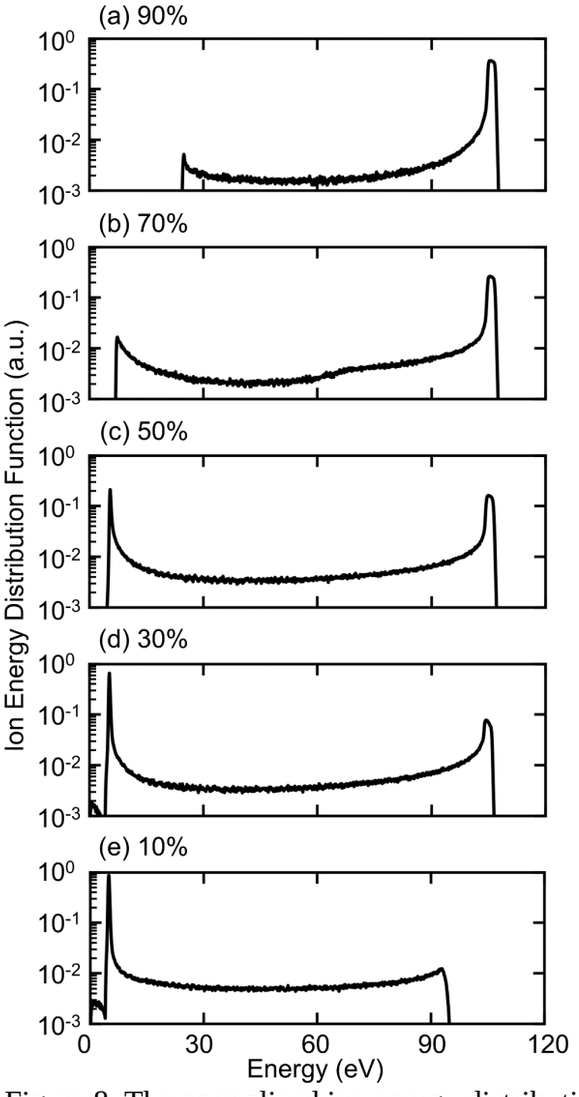

Figure 8. The normalized ion energy distribution function at duty cycle of (a) 90%, (b) 70%, (c) 50%, (d) 30%, and (e) 10%. These results are for Cl_2 plasma at 500 W ICP power and rectangular bias voltage.

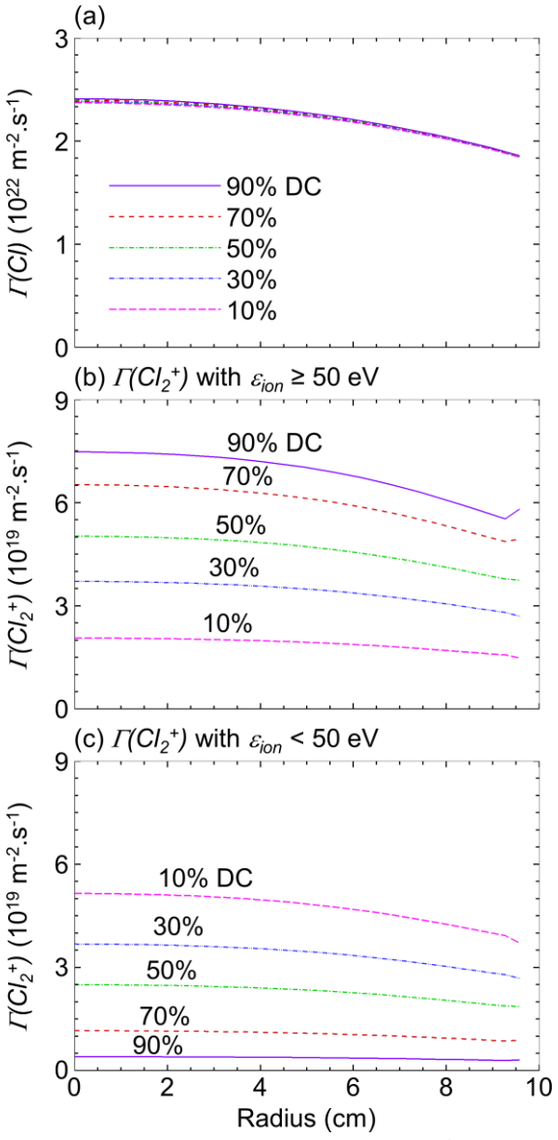

Figure 9. The flux of (a) Cl, (b) Cl_2^+ ions below 50 eV, and (c) Cl_2^+ ions with $\varepsilon_{ion} \geq 50$ eV at the bottom electrode. These fluxes have been plotted as a function of radius for duty cycle of 10 – 90%. These results are for Cl_2 plasma at 500 W ICP power, 10 mTorr, and rectangular bias voltage.

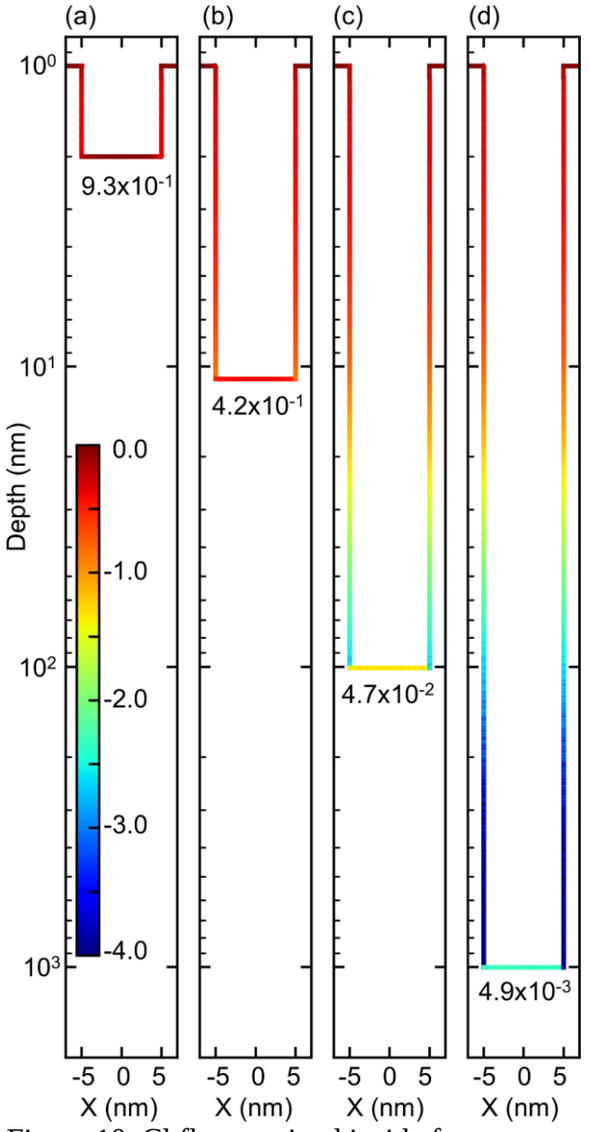

Figure 10. Cl flux received inside four rectangular trenches with aspect ratios of 0.1 (a), 1 (b), 10 (c), and 100 (d), assuming a sticking coefficient of one. The color lines show the geometries of the four aspect ratio trenches. The color represents the common logarithm of the normalized flux, $log10\left(\Gamma_{Cl}\ (x,z)/\Gamma_{Cl,from\ plasma}\right)$. The number in each figure is the normalized flux values received at the bottom center of the trenches.

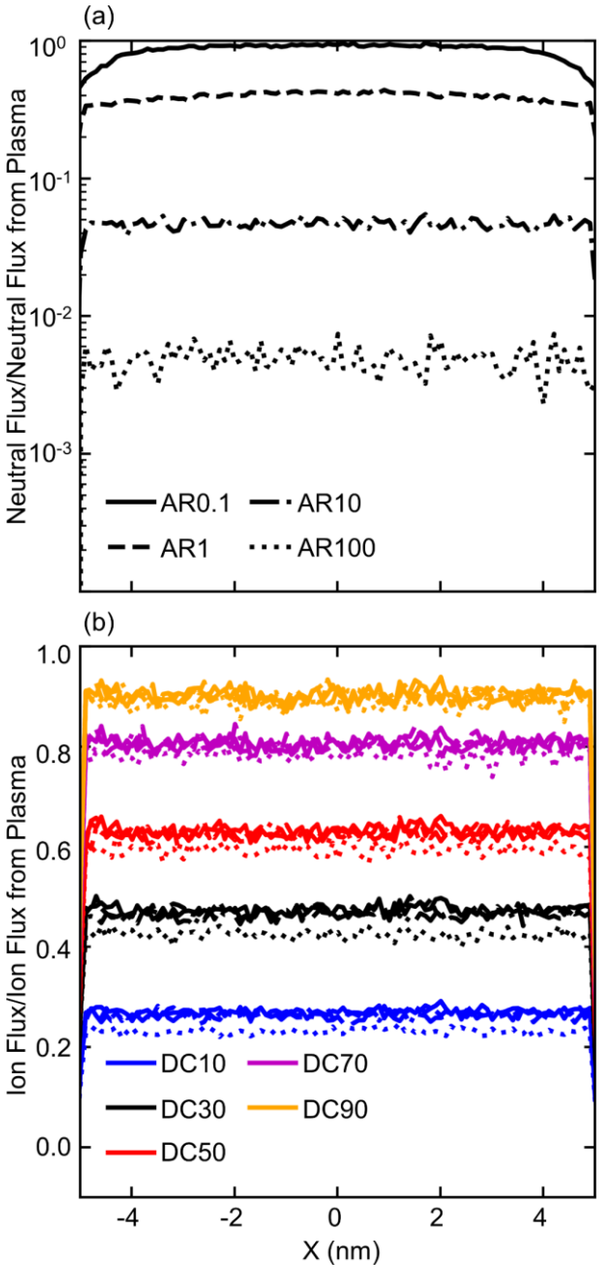

Figure 11. Normalized fluxes of (a) Cl and (b) Cl_2^+ with energy larger than 50 eV received at the bottom of the rectangular trenches. For both Cl and Cl_2^+, assume a sticking coefficient of one. The line type indicates the aspect ratio of the trenches, and the color of the lines indicates the bias voltage duty cycle.

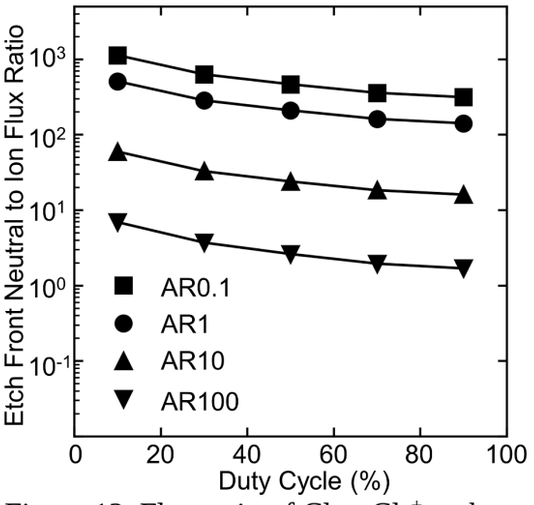

Figure 12. Flux ratio of Cl to Cl_2^+ at the etch front as a function of bias voltage duty cycle and aspect ratio. The lines are drawn to guide the eye.